THE JOURNAL OF PHYSICAL CHEMISTRY C

ARTICLE

pubs.acs.org/JPCC

Relative Stabilities of Low Index and Stepped CeO_2 Surfaces from Hybrid and GGA + *U* Implementations of Density Functional Theory

María M. Branda,[†] Ricardo M. Ferullo,[‡] Mauro Causà,[§] and Francesc Illas[⊥]

[†]Departamento de Física, Universidad Nacional del Sur, Bahía Blanca, Argentina

[‡]Departamento de Química, Universidad Nacional del Sur, Bahía Blanca, Argentina

[§]Dipartimento di Chimica, Universita' di Napoli Federico II, I-80126 Naples, Italy

[⊥]Departament de Química Física and Institut de Química Teòrica i Computacional (IQTCUB), Universitat de Barcelona, C/ Martí i Franquès 1, E-08028 barcelona, Spain

ABSTRACT: The relative stability of nine different well defined CeO_2 surfaces has been studied by periodic density functional calculations using GGA + *U* and B3LYP exchange-correlation functional. Both methods consistently predict that $CeO_2(111)$ is the most stable surface and also provide a consistent picture of the most stable surfaces which indeed are in agreement with previous studies based on empirical interatomic potentials. The facility of ceria surfaces to undergo a redox process has been investigated by forcing spin-polarized solutions, which lead to the occupancy of Ce 4f orbitals. These calculations provide evidence that surfaces with low-coordinated Ce cations are likely to be reduced more easily than regular low-index Miller surfaces.

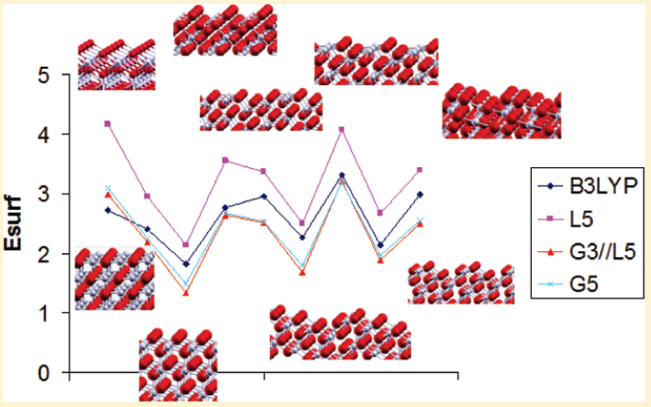

INTRODUCTION

The excellent performance of cerium oxide (or ceria) as an oxygen buffer has its origin in its distinctive combination of elevated oxygen transport capacity, redox ability to interchange rather easily Ce^{3+} and Ce^{4+} oxidation states, and compatibility with noble metals. These properties known since more than two decades ago[1,2] provide the basis of the so-called three-way catalysts (TWC), which requires an efficient oxygen buffer to convert toxic gases such as NO, CO, and hydrocarbons into harmless CO_2 and N_2. Ceria also exhibits the ability to regulate the oxygen partial pressure at several temperatures,[1,2,4] which coupled to the properties commented above have generated intense interest for other heterogeneous catalytic reactions, including several key applications in solid oxide fuel cells.[5,6] Because of its behavior as a good ionic conductor,[7,8] and at the same time as a good catalyst support for metal nanoparticles,[3,9] cerium oxide can be used both as an electrolyte and as an anode support. Interestingly, the catalytic properties of ceria become new and unique upon decreasing the size of ceria crystallites to the nanoscale. For example, Au clusters supported on ceria nanoparticles of ∼3−4 nm diameter exhibit an increase of 2 orders of magnitude in the CO oxidation rate with respect to the same reaction occurring when Au nanoparticles are supported on extended ceria surface.[10] A supply of reactive oxygen from the ceria nanoparticles has also been detected.[11]

The important technological applications of ceria have triggered a rather large number of studies addressing several aspects of both ceria bulk and surfaces both from theoretical[12−30] and experimental[31−38] points of view. From the point of theory, it is important to remark that, as in the case of several transition-metal oxides such as NiO,[39] the electronic structure of reduced ceria exhibits strong electron correlation effects, which are poorly described by the conventional local density approach (LDA) and generalized gradient approach (GGA) to the exchange correlation potential which is a necessary ingredient of density functional theory (DFT). Both LDA and GGA average the exchange correlation of the electronic interaction and do not correct for the unphysical self-interaction of the electrons arising from the classical Coulombic repulsion interelectronic potential. In the case of Ce_2O_3, or other reduced ceria CeO_{2-x} samples, the strongly localized Ce-4f band is partially occupied and hence the corresponding electronic structure is poorly described by LDA and GGA. To overcome the difficulties of LDA and GGA, it is necessary to make use of more sophisticated forms for the exchange correlation potential. A first approach consists in introducing a Hubbard like *U* term, which penalizes the situations where two electrons occupy a 4f orbital on a given Ce ion.

Received: December 1, 2010
Revised: January 11, 2011
Published: February 14, 2011

A second, in principle more accurate, approach consists in making use of hybrid functional including a part of nonlocal Fock exchange. The former approach introduces a direct correction to the 4f band (or 3d in the case of transition-metal oxides), whereas the latter modifies the whole electronic density. Nevertheless, both introduce some degree of empiricism because in one case a U value is needed, which is usually not provided by theory and, in the second one, a decision has to be made regarding the percent of Fock exchange added to the exchange potential.

The difficulties above-mentioned to describe the electronic structure of ceria also affect the description of ceria surfaces and their relative stability. In a pioneering article, Conesa[16] investigated the relative stability of several CeO_2 low Miller index surfaces of ceria based on the use of interatomic potentials (IP) and found that the relative order of stabilities was (111) > (110) > (211) > (100)/(210) > (310). Periodic Hartree−Fock calculations[17] also predict that the (111) surface is more stable than the (110) one. However, DFT calculations[18,19] performed on the (111), (110), and (100) surfaces using the GGA potential showed the same relative stabilities found by using the IP approximation: (111) > (110) > (100). The higher stability of the (111) surface was confirmed in X-ray photoemission spectroscopy (XPS) in combination with low-energy electron-diffraction (LEED) experiments.[14] Later on, Jiang et al.[22] reported a more systematic investigation including a larger number of well defined ceria surfaces. These authors reported perhaps the first LDA + U study of ceria surfaces. They used an U = 7 eV and J = 0.7 eV and have shown, not unexpectedly, that the LDA + U calculated surface energy of the stoichiometric CeO_2(111) surface is very close to that predicted by LDA. Rather recently, Fronzi et al.[40] reported GGA calculations for the low-index surfaces of CeO_2 for various terminations and surface defects. They found that the most stable surfaces for decreasing values of the chemical potential (i.e., for increasingly oxygen-lean conditions) are the stoichiometric CeO_2(111) surface, the CeO_2-(111) surface with subsurface oxygen vacancies, and the CeO_2(111)/Ce terminated surface.

From the above discussion, it is clear that whereas some advances have been made regarding our understanding of ceria surfaces, there is still a need for systematic study regarding the stability of low index and stepped ceria surfaces and, in particular, to compare result arising from GGA + U and hybrid functionals. This is an essential issue because describing the electronic structure of ceria, bulk, and surface is far from being a simple issue[21] although there is increasing evidence that GGA + U and hybrid approaches provide a similar picture, even for reduced ceria[41] and reduced ceria surfaces.[42] Nevertheless, there are still open questions regarding the choice of the best hybrid functional.[43] Furthermore, it is also imperative to establish whether different DFT methods coincide in the prediction of the relative stability of ceria surfaces. Finally, the description of ceria stepped is particularly important because they contain low-coordinate sites, which will exhibit a different reactivity as is the case for oxygen vacancy formation on ceria nanoparticles.[44,45] The precise knowledge of the stability of the stepped surfaces also provides a proper reference limit for ceria nanoparticles where size has been shown to play a role.[44,45] In the following, we present a detailed systematic study of a rather large number of CeO_2 faces as predicted from hybrid DFT, using the broadly employed B3LYP exchange and correlation potential, and from DFT with the on-site Hubbard correction (LDA + U and GGA + U). We will show that these approaches provide a rather coincident picture of the stability of ceria surfaces and, more importantly, of their redox capability.

COMPUTATIONAL DETAILS

The electronic and geometrical structures for the hybrid density functional calculations with the B3LYP functional[46,47] have been obtained using parallel and massive parallel versions of the *CRYSTAL06* program[48] whereas the geometrical analysis of the surfaces has been performed using a modified version of the *CRYSTAL98* program.[49] Calculated values have always been checked for convergence against numerical control parameters. The maximum point symmetry has been employed for the slab models. The effect of the Ce core electrons on the valence electronic structure has been taken into account through a relativistic small core effective core potential[50] and a valence basis set was optimized starting from the segmented Gaussian Type Orbital (GTO) basis set reported by Cao and Dolg.[51] The basis set for f orbitals has been optimized on Ce_2O_3 bulk model and then adopted in all calculations of CeO_2 bulk and surfaces. The oxygen basis set was taken from Towler et al.[52]

However, periodic density functional calculations within the LDA + U and GGA + U potentials[53−55] have been carried out employing the Vienna Ab-initio Simulation Package (VASP).[56−58] In this case, the effect of the core electrons is taken into account by means of the projector augmented wave (PAW) method[59] and the valence electron density expanded in a plane wave basis. The U values for LDA + U and GGA + U were taken from a previous work about bulk CeO_2 and Ce_2O_3,[60] namely, U_{eff} = 5 eV for LDA + U and U_{eff} = 3 eV for GGA + U. The VWN66 and PW91 exchange-correlation forms of the LDA and GGA potentials have been chosen[61,62] together with the formalism of Dudarev et al.[63] for the introduction of the U term. Note that the GGA + U method leads to acceptable agreement with experiment at lower U_{eff} energies than those necessary in the LDA + U method[60] because of the more accurate treatment of correlation effects within the GGA potential. However, the CeO_2 structural properties, such as lattice constants and bulk modulus are somewhat better represented by the LDA + U method.[60] Therefore, geometry optimization has been performed throughout within the LDA + U scheme, whereas energies and magnetic moments have been calculated by a GGA(PW91) + U approach. Extensive test calculations have shown that a cutoff of 415 eV for the kinetic energy of the plane waves in the basis set allowed a convergence up to 10^{-4} eV in the total energy. The numerical integrations in the corresponding 2D Brillouin zone were performed on a grid of 4 × 4 × 1 Monkhorst−Pack special k-points.[64] The Methfessel−Paxton smearing of width σ = 0.05 eV was applied and the reported total energies were then extrapolated to $\sigma \rightarrow 0$ eV.[65] All of the calculations were performed at the spin-polarized and nonpolarized level. The total energy threshold defining self-consistency of the electron density was set to 10^{-4} eV and the convergence criterion for structural optimization was set to be a total energy difference less than 10^{-3} eV for consecutive geometries.

SURFACE MODELS

LDA + U, GGA + U, and B3LYP periodic density functional calculations as described in the previous section have been carried out for a series of slab models that represent nine different CeO_2 surfaces. In all cases, the surface was represented by a

periodic slab model although it is important to remark that B3LYP calculations use a real 2D slab model, whereas the LDA + U and GGA + U calculations are carried out by means of the repeated slab model, which is unavoidable when using a delocalized, periodic, basis set. In this case, a sufficiently wide vacuum width between the repeated slabs is necessary to avoid spurious interaction between the repeated slabs. Test calculations show that a width of 12 Å provides converged values. Hence, slab models containing up to 27 atomic layers were selected with a vacuum width of ∼12 Å between the interleaved slabs. The same models but without the vacuum width were employed in the B3LYP calculations.

Slab models representing the (100), (110), (111), (210), (211), (221), (311), (331), and (531) perfect surfaces were built from the CeO_2 bulk cubic (Fm3m) CaF_2 structure. All surfaces are oxygen terminated. Note that within this crystal structure it is not possible to define any cation terminated slab model without breaking stoichiometry. The geometrical structures were always fully optimized using hybrid B3LYP, LDA + U (U = 5 eV; hereafter referred to as L5), and GGA + U (U = 5 eV, hereafter referred to as G5) with the optimized lattice parameter values: a_0 = 5.45, 5.40, and 5.47 Å, respectively, which compare relatively well with the experimental value of a_0 = ∼5.41 Å (5.406(1) Å[66] or 5.411(1) Å[67]). Calculations carried out at the L5 geometry but with the G3 functional are indicated as G3//L5 as in previous work.[68,69] This latter strategy attempts at using the L5 geometry, which is closer to experiment while computing the energy from an, in principle, better (G3) functional.

RESULTS AND DISCUSSION

The optimized structures of the nine CeO_2 studied faces are schematically shown in Figure 1. The analysis of the geometrical structures reveal that, for the faces with lower Miller indexes, namely (100), (110), and (111) there are practically no appreciable changes in the interatomic distances. However, this is not the case for the faces with larger Miller indexes. In the case of L5 calculations, these changes are ∼±0.2 Å for the Ce−Ce and Ce−O distances with respect to the bulk distances of 3.82 and 2.34 Å, respectively.

Surface energies calculated with the different approaches are summarized in Table 1; this includes the results obtained from the B3LYP, L5, and G3 methods as well as results obtained from the mixed G3//L5 approach. Table 1 shows that all methods consistently predict the (111) face as the most stable termination of CeO_2, in accord with previous results from interatomic potentials[16] or from GGA + U density functional calculations.[22] Moreover, the four more stable surfaces predicted by all approaches are the same except for an interchange between the second and third most stable ones where B3LYP prefers (331) and GGA + U prefers (221). Nevertheless, the difference in surface energy between these two faces is very small (less than 0.2 eV) and probably within the limits of accuracy of the present density functional approaches. Note also that the differences in geometrical structure between (331) and (221) surfaces are also very small (Figure 1). However, the order (111) > (110) > (211) > (210) > (100) obtained by our LDA + U and GGA + U calculations is in accord with the results of Conesa[16] and also agrees with those of Jiang et al.[22] This is clearly seen from Table 2 reporting the order of stability predicted by present and previous studies. Note, however, that previous studies did not consider the

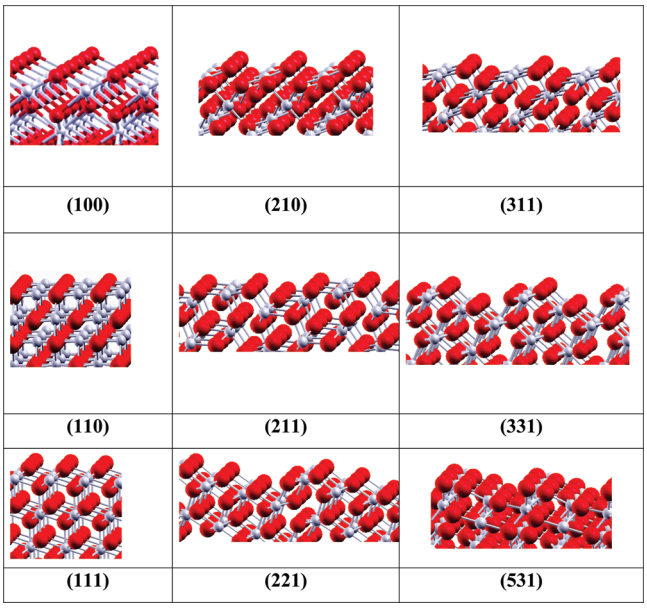

Figure 1. Sketches (side view) of the optimized CeO_2 surface slab models corresponding to the nine studied faces (Color online: small gray spheres and large red spheres correspond to Ce cations and O anions, respectively).

Table 1. Calculated Interplane Distances (d_{hkl} in Angstroms) and Surface Energy Values (E_{surf} in J m^{-2}) for the Nine Different Faces of CeO_2 Studied in the Present Work; the Values are Listed According to the Order of Stability Predicted by the B3LYP Periodic Calculations and the Values in Parenthesis Provide the Order of Stability for a Given Method

		E_{surf}			
surface	d_{hkl}	B3LYP[a]	L5[b]	G3//L5[c]	G5[d]
(111)	**3.15**	**1.83 (1)**	**2.14 (1)**	**1.33 (1)**	**1.49 (1)**
(331)	**1.25**	**2.14 (2)**	**2.68 (3)**	**1.88 (3)**	**1.97 (3)**
(221)	**0.91**	**2.26 (3)**	**2.50 (2)**	**1.68 (2)**	**1.80 (2)**
(110)	1.93	2.40 (4)	2.96 (4)	2.18 (4)	2.25 (4)
(100)	2.73	2.72 (5)	4.16 (9)	2.99 (8)	3.09 (8)
(210)	1.22	2.77 (6)	3.56 (7)	2.64 (7)	2.67 (7)
(211)	1.11	2.95 (7)	3.36 (5)	2.52 (6)	2.53 (5)
(531)	0.92	2.98 (8)	3.39 (6)	2.50 (5)	2.54 (6)
(311)	1.64	3.31 (9)	4.07 (8)	3.21 (9)	3.19 (9)

[a] Calculations carried out using the B3LYP optimized a_0 value of 5.45 Å. [b] Calculations carried out using the L5 optimized a_0 value of 5.40 Å. [c] Single-point calculations at the L5 optimized geometry. [d] Calculations carried out using the G5 optimized a_0 value of 5.47 Å.

(331) and (221) faces which are very stable surfaces and likely to be present on ceria nanoparticles. In addition to the results presented by Conesa[16] and by Jiang et al.,[22] the present study found that, according to the LDA + U and GGA + U methods, the (100) face is one of the least stable surfaces. Nevertheless, our B3LYP results found this face more stable than (211) and (210). Moreover, we can observe that, not surprisingly, the values of the surface energy obtained using G3//L5 and G5 are in close agreement with results reported by Jiang et al.[22]

Table 2. Order of Stability of the Difference Surfaces of CeO_2 as Predicted by Present and Previous Studies

IP[a]	(111) > (110) > (211) > (210) ~ (100)
G5[b]	(111) > (110) > (210) > (211) > (100)
B3LYP[c]	(111) > (331) > (221) > (110) > (100) > (210) > (211) > (531) > (311)
L5[c]	(111) > (221) > (331) > (110) > (211) > (531) > (210) > (311) > (100)
G5[c]	(111) > (221) > (331) > (110) > (211) > (531) > (210) > (100) > (311)
G3//L5[c]	(111) > (221) > (331) > (110) > (531) > (211) > (210) > (100) > (311)

[a] Interatomic potentials, ref 16. [b] Ref 22. [c] This work.

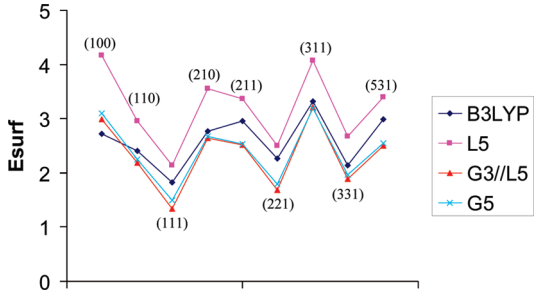

Figure 2. Evolution of surface formation energy, E_{surf}, with respect to the surface Miller indexes.

Table 3. Relative Stability of Open-Shell Triplet State Versus Closed-Shell Ground State (Δ in eV) and Population of the 4f Orbital of the Surface Ce Cations (N_f) on the Spin-Polarized Solutions as Predicted from B3LYP and L5 Calculations[a]

	B3LYP		L5	
surface	Δ	N_f	Δ	N_f
(111)	1.56	0.35	1.24	0.28
(331)	1.29	0.50	0.88	0.56
(221)	1.31	0.49	0.89	0.56
(110)	1.27	0.50	0.81	0.57
(100)	1.50	0.27[b]	1.25	0.55
(210)	1.38	0.52	1.01	0.54
(211)	1.21	0.53	0.96	0.54[b]
(531)	1.10	0.51[b]	1.02	0.52[b]
(311)	1.19	0.51[b]	0.99	0.55

[a] Note that Δ correspond to the energy difference between spin-polarized and spin-unpolarized energies divided by 2 to take the presence of 2 surfaces into account and that the order in the table follows the stability order found with hybrid calculations. [b] Spin not localized on the most external Ce atom.

To provide a clue concerning the predicted surface stability order, the surface energy values following increasing order for Miller indexes on the abscissa are drawn in Figure 2. As it can be observed, the E_{surf} values are little affected by the choice of the U parameter, in agreement with the results of Jiang et al.[22] Moreover, the same curve is found for results arising from either LDA + U or GGA + U calculations and the curve corresponding to hybrid B3LYP calculations follows the same trend. The only discrepancy again is the position of E_{surf} value of (100) face, which is considerably more stable for hybrid calculations than for the LDA + U or GGA + U ones. However, the surface energy values obtained with hybrid calculations are placed between LDA + U and GGA + U, the latter being larger and the former smaller than hybrid B3LYP values, which provides reasonable errors bars for the calculated surface energy values.

Table 4. Mulliken Atomic Net Charges for Bulk Structures and Slab Models as Predicted from Periodic B3LYP Calculations for the Closed-Shell (Singlet) and Spin-Polarized Solutions (SP) with Two Unpaired Electrons Per Unit Cell

		Bulk O	Bulk Ce	Surf O	Surf Ce
CeO_2	singlet	−1.43	2.85		
Ce_2O_3	SP	−1.72, −1.77	2.61		
(111)	singlet	−1.43	2.87	−1.36	2.81
	SP	−1.43	2.87	−1.32	2.75
(331)	singlet	−1.43	2.86	−1.36	2.72
	SP	−1.43	2.86	−1.32	2.63
(221)	singlet	−1.44	2.86	−1.35	2.72
	SP	−1.43	2.84	−1.33	2.63
(110)	singlet	−1.44	2.87	−1.32	2.71
	SP	−1.44	2.87	−1.27	2.62
(100)	singlet	−1.42	2.86	−1.22	2.69
	SP	−1.42	2.86	−1.15	2.64
(210)	singlet	−1.40	2.85	−1.20	2.59
	SP	−1.40	2.85	−1.12	2.51
(211)	singlet	−1.44	2.85	−1.39	2.52
	SP	−1.43	2.85	−1.37	2.50
(531)	singlet	−1.45	2.83	−1.16	2.59
	SP	−1.45	2.83	−1.09	2.58
(311)	singlet	−1.44	2.87	−1.13	2.53
	SP	−1.44	2.87	−1.08	2.53

To further analyze the effect of surface termination on the electronic structure of the resulting systems, calculations have been carried out for a spin-polarized solution with two unpaired electrons per unit cell. The ground state corresponds always to the closed-shell (spin unpolarized) solution but the energy difference between these two states provides information about the relative facility to reduce surface Ce^{4+} cations to the Ce^{3+} oxidation state. The idea behind the spin-polarized calculations is to artificially force the occupancy of the Ce 4f orbitals and, hence, to obtain an estimate of the energy cost necessary for such a redox process and thus provide information about the reducibility of the different CeO_2 surfaces studied in the present work. The total energy differences between spin-polarized (triplet like) and closed-shell (singlet) states and the 4f populations on a surface Ce atom corresponding to the spin-polarized solution are displayed in Table 3. For the (111) and (100) faces, singlet states are 1.25 eV (LDA + U) and 1.56 eV (B3LYP) more stable than triplet states. In these cases, there are not Ce^{3+} surface ions.

dx.doi.org/10.1021/jp111427j |J. Phys. Chem. C 2011, 115, 3716–3721

Table 5. Mulliken Atomic Spin Densities for Bulk Structures and Slab Models as Predicted from Periodic B3LYP Calculations for the Spin-Polarized Solutions (SP) with Two Unpaired Electrons Per Unit Cell[a]

	bulk O	bulk Ce	surf O	surf Ce	4f pop.
Ce_2O_3					1
(111)	0.01	0.02	0.22	0.34	0.35
(331)	0	0	0.18	0.50	0.50
(221)	0.05	0.02	0.14	0.49	0.49
(110)	0	0	0.23	0.50	0.50
(100)	0.01	0.08	0.27	0.27	0.27
(210)	0	0	0.31	0.54	0.52
(211)	0.02	0	0.36	0.52	0.53
(531)	0.02	0	0.24	0.52	0.51
(311)	0.01	0	0.15	0.51	0.51

[a] Note that the spin density is mostly localized on external Ce atoms, with totally *4f* character although neighboring O atoms bear a noticeably spin density.

However, this energy difference decreases up to 0.81 eV (LDA + *U*) and 1.10 eV (B3LYP) for the faces with low-coordinated surface sites (Table 3) in agreement with previous studies suggesting that low-coordinated sites on stepped ceria surfaces are more easily reduced than the regular sites.[20] It is also important to notice that, once again, one can observe a good agreement between LDA + *U* and B3LYP results. Finally, Tables 4 and 5 report atomic net charges and atomic spin densities from a Mulliken population analysis carried out for the B3LYP spin-polarized solutions. To have a better comparison the population analysis was calculated for the bulk and for the different surface models. These results show that bulk values are well reproduced for the atoms at the center of the slab models. In fact, the inner inside Ce and O atoms of the slabs have the same atomic charges as the ones in CeO_2 bulk. The values on Tables 4 and 5 also show that the surface is less ionic than the bulk, as usual and that the atomic net charges of surface Ce atoms are very close to those on Ce_2O_3 bulk with the exception of (111) surface. Note also that for (111), (221), (331), (210), (110) spin is localized on most external (surface) Ce atom whereas for (100), (531), (311), (211) spin is localized on subsurface Ce atom depending on the approach used. It is also important to point out that, even if most of the spin density is localized in the reduced Ce atoms, there is also a considerable spin density in the neighboring O atoms. However, this is likely to be an artifact from the Mulliken population analysis and from the fact that Ce^{3+} has a larger size, which makes that its electron density is closer to the O anions and partly described by the GTO basis functions centered in those atoms.

CONCLUSIONS

Periodic density functional calculations within two different approaches which go beyond the standard LDA and GGA exchange-correlation functionals have been carried out to study the relative stability of nine different well defined CeO_2 surfaces. All methods consistently predict that CeO_2(111) is the most stable surface. In addition, for the most stable surfaces the different methods provide also a consistent picture with small variations in the prediction of the second and third most stable surface although mainly due to the small difference in the calculated surface energies. Moreover, the order of stability predicted by these state of the art density functionals is in agreement with predictions from simple interatomic potentials evidencing the usefulness of this approach to investigate the atomic structure of extended ceria surfaces but also of ceria nanoparticles. This is a strategy that is currently being used to provide reasonable structures of ceria nanoparticles, at least as a starting point for density functional calculations.[70,71]

The capability of different ceria surfaces to undergo a redox process has been investigated by forcing spin-polarized solutions, which lead to the occupancy of Ce 4f orbitals. Even if these calculations predict that the ground state is always of closed-shell type, they provide evidence that surfaces with low-coordinated Ce cations are likely to be reduced more easily than regular low-index Miller surfaces, a conclusion that is also in agreement with previous findings using different models of stepped ceria surfaces.

Finally, the overall very good agreement between results from LDA + *U* or GGA + *U* approaches and the hybrid B3LYP functional is remarkable and, in line with recent studies,[41−43] strongly suggesting that the former, less computationally demanding when used within a plane wave basis set, approaches provide a valid description of ceria surfaces and, probably, of chemisorptions or reactivity thereon.

ACKNOWLEDGMENT

M.C. is grateful for financial support to his visit to Barcelona through the HPC-Europa project and F.I. acknowledges support through the ICREA ACADEMIA award. Financial support by the Spanish MICINN (grants FIS2008-02238, CTQ2007-30547-E/BQU, CTQ2009-07647/BQU), Generalitat de Catalunya (grants 2009SGR1041 and XRQTC) is gratefully acknowledged. Computational time has been generously provide by the Barcelona Supercomputing Center

REFERENCES

(1) Yao, H. C.; Yu, Y. F. *J. Catal.* **1984**, *86*, 254.
(2) Taylor, K. C. *Catalysis Science and Technology*; Anderson, J. R., Boudart, M., Eds.; Springer: Berlin, 1984; Vol. 5.
(3) Trovarelli, A. *Catal. Rev.−Sci. Eng.* **1996**, *38*, 439.
(4) Taylor, K. C. *Catal. Rev.−Sci. Eng.* **1993**, *35*, 3457.
(5) Dresselhaus, M. S.; Thomas, I. L. *Nature* **2001**, *414*, 332.
(6) Esposito, V.; Traversa, E. *J. Am. Ceram. Soc.* **2008**, *91*, 1037.
(7) Saraf, L.; Wang, C. M.; Shutthanandan, V.; Zhang, Y.; Marina, O.; Baer, D.; Thevuthasan, S.; Nachimuthu, P.; Lindle, D. *J. Mater. Res.* **2005**, *20*, 1295.
(8) Kim, S.; Maier, J. *J. Eur. Ceram. Soc.* **2004**, *24*, 1919.
(9) Trovarelli, A. *Catal. Sci.* **2002**, *2*, 407.
(10) Carrettin, S.; Concepcion, P.; Corma, A.; Nieto, J. M. L.; Puntes, V. F. *Angew. Chem., Int. Ed.* **2004**, *43*, 2538.
(11) Guzman, J.; Carrettin, S.; Corma, A. *J. Am. Chem. Soc.* **2005**, *127*, 3286.
(12) Perrichon, V.; Laachir, A.; Abournadasse, S.; Tourer, O.; Blanchard, G. *Appl. Catal., A* **1995**, *129*, 69.
(13) Terribile, D.; Trovarelli, A.; Llorca, J.; Leitenburg, C. de; Dolcetti, G. *J. Catal.* **1998**, *178*, 299.
(14) Siokou, A.; Nix, R. M. *J. Phys. Chem. B* **1999**, *103*, 6984.
(15) Sayle, T. X. T.; Parker, S. C.; Catlow, C. R. A. *Surf. Sci.* **1994**, *316*, 329.
(16) Conesa, J. C. *Surf. Sci.* **1995**, *339*, 337.
(17) Gennard, S.; Cora, F.; Catlow, C. R. A. *J. Phys. Chem. B* **1999**, *103*, 10158.
(18) Skorodumova, N. V.; Baudin, M.; Hermansson, K. *Phys. Rev. B* **2004**, *69*, 075401.

(19) Yang, Z.; Woo, T. K.; Baudin, M.; Hermansson, K. *J. Chem. Phys.* **2004**, *120*, 7741.
(20) Branda, M. M.; Loschen, C.; Neyman, K. M.; Illas, F. *J. Phys. Chem. C* **2008**, *112*, 17643.
(21) Ganduglia-Pirovano, M. V.; Hofmann, A.; Sauer, J. *Surf. Sci. Rep.* **2007**, *62*, 219.
(22) Jiang, Y.; Adams, J. B.; van Schilfgaarde, M. *J. Chem. Phys.* **2005**, *123*, 064701.
(23) Loschen, C.; Carrasco, J.; Neyman, K. M.; Illas, F. *Phys. Rev. B* **2007**, *75*, 035115.
(24) Da Silva, J. L. F. *Phys. Rev. B* **2007**, *76*, 193108.
(25) Andersson, D. A.; Simak, S. I.; Johansson, B.; Abrikosov, I. A.; Skorodumova, N. V. *Phys. Rev. B* **2007**, *75*, 035109.
(26) Pacchioni, G. *J. Chem. Phys.* **2008**, *128*, 182505.
(27) Castleton, C. W. M.; Kullgren, J.; Hermansson, K. *J. Chem. Phys.* **2007**, *127*, 244704.
(28) Hay, P. J.; Martin, R. L.; Uddin, J.; Scuseria, G. E. *J. Chem. Phys.* **2006**, *125*, 034712.
(29) Voloshina, E.; Paulus, B. *J. Chem. Phys.* **2006**, *124*, 234711.
(30) Da Silva, J. L. F.; Ganduglia-Pirovano, M. V.; Sauer, J. *Phys. Rev. B* **2007**, *75*, 045121.
(31) Pfau, A.; Schierbaum, K. D. *Surf. Sci.* **1994**, *321*, 71.
(32) Wuilloud, E.; Delley, B.; Schneider, W. D.; Baer, Y. *Phys. Rev. Lett.* **1984**, *53*, 202.
(33) Mullins, D. R.; Overbury, S. H.; Huntley, D. R. *Surf. Sci.* **1998**, *409*, 307.
(34) Holgado, J. P.; Alvarez, R.; Munuera, G. *Appl. Surf. Sci.* **2000**, *161*, 301.
(35) Wang, S. Y.; Qiao, Z. P.; Wang, W.; Qian, Y. T. *J. Alloys Compd.* **2000**, *305*, 12.
(36) Garvie, L. A. J.; Buseck, P. R. *J. Phys. Chem. Solids* **1999**, *60*, 1943.
(37) Fujimori, A. *Phys. Rev. Lett.* **1984**, *53*, 2518.
(38) Esch, F.; Fabris, S.; Zhou, L.; Montini, T.; Africh, C.; Comelli, P.; Rosei, R. *Science* **2005**, *309*, 752.
(39) Moreira, I.; de, P. R.; Illas, F.; Martin, R. L. *Phys. Rev. B* **2002**, *65*, 155102.
(40) Fronzi, M.; Soon, A.; Delley, B.; Traversa, E.; Stampfl, C. *J. Chem. Phys.* **2009**, *131*, 104701.
(41) Kullgren, J.; Castleton, C. W. M.; Müller, C.; Muñoz Ramo, D.; Hermansson, K. *J. Chem. Phys.* **2010**, *132*, 054110.
(42) Nolan, M. *Chem. Phys. Lett.* **2010**, *499*, 126.
(43) Graciani, J.; Marquez, A. M.; Plata, J. J.; Ortega, Y.; Hernandez, N. C.; Meyer, A.; Zicovich-Wilson, C. M.; Sanz, J. F. *J. Chem. Theory Comput.*, in press (D.O.I. 10.1021/ct100430q).
(44) Migani, A.; Vayssilov, G. N.; Bromley, S. T.; Illas, F.; Neyman, K. M. *Chem. Commun.* **2010**, 5936.
(45) Migani, A.; Vayssilov, G. N.; Bromley, S. T.; Illas, F.; Neyman, K. M. *J. Mater. Chem.* **2010**, *20*, 10535.
(46) Becke, A. D. *J. Chem. Phys.* **1993**, *98*, 5548.
(47) Lee, C.; Yang, W.; Parr, R. G. *Phys. Rev. B* **1998**, *37*, 785.
(48) Dovesi, R.; Saunders, V. R.; Orlando, R.; Zicovich-Wilson, C. M. ; Pascale, F.; Civalleri, B.; Doll, K.; Bush, I. J.; D'Arco, P. ; Lunell, M. *Crystal 2006 User Manual*; Turin University: Turin, 2007.
(49) Saunders, V. R. ; Dovesi, R.; Roetti, C.; Causà, M.; Harrison, N. M. ; Orlando, R.; Zicovich-Wilson, C. M. *CRYSTAL98 User's Manual*, University of Torino: Torino, 1998.
(50) Dolg, M.; Stoll, H.; Preuss, H. *J. Chem. Phys.* **1989**, *90*, 1730.
(51) Cao, X.; Dolg, M. *J. Mol. Struct. Theochem.* **2002**, *581*, 139.
(52) Towler, M. D.; Allan, N. L.; Harrison, N. M.; Saunders, V. R.; Mackrodt, W. C.; Apra, E. *Phys. Rev. B* **1994**, *50*, 5041.
(53) Anisimov, V. I.; Aryasetiawan, F.; Lichtenstein, A. I. *J. Phys.: Condens. Matter* **1997**, *9*, 767.
(54) Anisimov, V. I.; Solovyev, I. V.; Korotin, M. A.; Czyzyk, M. T.; Sawatzky, G. A. *Phys. Rev. B* **1993**, *48*, 16929.
(55) Solovyev, I. V.; Dederichs, P. H.; Anisimov, V. I. *Phys. Rev. B* **1994**, *50*, 16861.
(56) Kresse, G.; Hafner, J. *Phys. Rev. B* **1993**, *47*, 558.
(57) Kresse, G.; Hafner, J. *Phys. Rev. B* **1993**, *48*, 13115.
(58) Kresse, G.; Hafner, J. *Phys. Rev. B* **1994**, *49*, 14251.
(59) Blöchl, P. E. *Phys. Rev. B* **1994**, *50*, 17953.
(60) Loschen, C.; Carrasco, J.; Neyman, K. M.; Illas, F. *Phys. Rev. B* **2007**, *75*, 035115.
(61) Perdew, J. P.; Chevary, J. A.; Vosko, S. H.; Jackson, K. A.; Pederson, M. R.; Singh, D. J.; Fiolhais, C. *Phys. Rev. B* **1992**, *46*, 6671.
(62) Perdew, J. P.; Chevary, J. A.; Vosko, S. H.; Jackson, K. A.; Pederson, M. R.; Singh, D. J.; Fiolhais, C. *Phys. Rev. B* **1993**, *48*, 4978.
(63) Dudarev, S. L.; Botton, G. A.; Savrasov, S. Y.; Humphreys, C. J.; Sutton, A. P. *Phys. Rev. B* **1998**, *57*, 1505.
(64) Monkhorst, H. J.; Pack, J. D. *Phys. Rev. B* **1976**, *13*, 5188.
(65) Methfessel, M.; Paxton, A. T. *Phys. Rev. B* **1989**, *40*, 3616.
(66) Duclos, S. J.; Vohra, Y. K.; Ruoff, A. L.; Jayaraman, A.; Espinosa, G. P. *Phys. Rev. B* **1998**, *38*, 7755.
(67) Gerward, L.; Olsen, J. S. *Powder Diffr.* **1993**, *8*, 127.
(68) Castellani, N. J.; Branda, M. M.; Neyman, K. M.; Illas, F. *J. Phys. Chem. C* **2009**, *113*, 4948.
(69) Branda, M. M.; Castellani, N. J.; Grau-Crespo, R.; de Leeuw, N. H.; Hernandez, N. C.; Sanz, J. F.; Neyman, K. M.; Illas, F. *J. Chem. Phys.* **2009**, *131*, 094702.
(70) Loschen, C.; Migani, A.; Bromley, S. T.; Illas, F; Neyman, K. M. *Phys. Chem. Chem. Phys.* **2008**, *10*, 5730.
(71) Migani, A.; Neyman, K. M.; Illas, F.; Bromley, S. T. *J. Chem. Phys.* **2009**, *131*, 064701.